Ultrasonics Sonochemistry 21 (2014) 324–335

Contents lists available at SciVerse ScienceDirect

Ultrasonics Sonochemistry

journal homepage: www.elsevier.com/locate/ultson

Sonochemical and high-speed optical characterization of cavitation generated by an ultrasonically oscillating dental file in root canal models

R.G. Macedo [a,*], B. Verhaagen [b], D. Fernandez Rivas [c], J.G.E. Gardeniers [c], L.W.M. van der Sluis [d], P.R. Wesselink [a], M. Versluis [b]

[a] Department of Cariology, Endodontology & Pedodontology, Academic Center for Dentistry Amsterdam, University of Amsterdam and VU University, Gustav Mahlerlaan 3004, 1081LA Amsterdam, The Netherlands
[b] Physics of Fluids Group and Institute for Biomedical Technology and Technical Medicine MIRA, University of Twente, P.O. Box 217, 7500AE Enschede, The Netherlands
[c] Mesoscale Chemical Systems Group, MESA+ Research Institute, University of Twente, P.O. Box 217, 7500AE Enschede, The Netherlands
[d] Department of Conservative Dentistry and Endodontics, Paul Sabatier University, 3 chemin des Maraîchers, 31062 Toulouse, France

ARTICLE INFO

Article history:
Received 24 September 2012
Received in revised form 25 February 2013
Accepted 2 March 2013
Available online 2 April 2013

Keywords:
Dentistry
Endodontics
Ultrasonic cleaning
Cavitation
Sonoluminescence
Sonochemiluminescence

ABSTRACT

Ultrasonically Activated Irrigation makes use of an ultrasonically oscillating file in order to improve the cleaning of the root canal during a root canal treatment. Cavitation has been associated with these oscillating files, but the nature and characteristics of the cavitating bubbles were not yet fully elucidated. Using sensitive equipment, the sonoluminescence (SL) and sonochemiluminescence (SCL) around these files have been measured in this study, showing that cavitation occurs even at very low power settings. Luminol photography and high-speed visualizations provided information on the spatial and temporal distribution of the cavitation bubbles. A large bubble cloud was observed at the tip of the files, but this was found not to contribute to SCL. Rather, smaller, individual bubbles observed at antinodes of the oscillating file with a smaller amplitude were leading to SCL. Confinements of the size of bovine and human root canals increased the amount of SL and SCL. The root canal models also showed the occurrence of air entrainment, resulting in the generation of stable bubbles, and of droplets, near the air–liquid interface and leading eventually to a loss of the liquid.

1. Introduction

Ultrasound is frequently used in dentistry in a wide range of therapeutic applications. Examples are the cleaning and disinfection of the inner and outer surface of a tooth, termed root canal therapy and periodontal scaling, respectively [1]. Ultrasonic agitation of disinfecting solutions in the root canal is called Ultrasonically Activated Irrigation (UAI) [2]. It has been shown to improve the chemical and mechanical efficiency of root canal cleaning procedures [2,3] and it promotes organic tissue dissolution during endodontic therapy [4]. In UAI an endodontic instrument is driven at 30 kHz and it has been shown to induce acoustic microstreaming and cavitation. These two phenomena are claimed to be the working mechanisms of ultrasonic irrigation [5–7].

The occurrence of cavitation during UAI has been discussed frequently over the past two decades. Cavitation has been demonstrated to occur around ultrasonically oscillating endodontic instruments in an unbounded medium [7–13]. Ahmad et al. [9] argued that cavitation is unlikely to occur inside the root canal, because space restrictions limit the amplitude of oscillation of the endodontic file. In a recent article [14], however, cavitation was shown to occur around the tip of an ultrasonically oscillating file, even within the confinement of a root canal, although only at high driving powers that are not commonly used clinically. Cavitation may also cause the enhancement of sonochemical reactions around dental scalers [7]. However, no clear data on the number, size, location and nature of cavitating bubbles during UAI exists. Furthermore, it is unclear how the confinement of the root canal affects the formation of cavitating bubbles.

Other than in pure liquids, cavitation is typically generated from nuclei, small pockets of air trapped in hydrophobic dirt particles or crevices in a wall. Bubbles can grow when the applied pressure drops below the ambient pressure minus the vapor pressure of the liquid [15,16]. The negative pressure needs to be generated by the oscillating endodontic file, similar to hydrodynamic cavitation which is known to occur for ship propellers and pumps[11,17–19]. The file moves with an oscillatory velocity $U = 2\pi fA$ (with f the oscillation frequency and A the amplitude of oscillation) and the fluid around the file is assumed to have a similar velocity. Near the trailing edge of the file, the fluid velocity equals zero, leading to low-pressure areas there [20]. The potential for cavitation to be generated is then characterized by the cavitation number Ca [15]:

* Corresponding author. Tel.: +31 614481420.
E-mail address: r.macedo@acta.nl (R.G. Macedo).

1350-4177/$ - see front matter © 2013 Elsevier B.V. All rights reserved.
http://dx.doi.org/10.1016/j.ultsonch.2013.03.001

$$Ca = \frac{P_{\text{ambient}} - P_{\text{vapor}}}{\frac{1}{2}\rho U^2} \quad (1)$$

where ρ is the density of the liquid. Under the condition that nuclei with radii larger than a critical radius are available, cavitation can occur when $Ca < 1$, for which the velocity needs to exceed 15 m/s [15] in water. The typical frequency of oscillation for endodontic devices is 30 kHz, thus the threshold oscillation amplitude is approximately 80 μm. This is a value that endodontic devices are able to reach at high power settings [21,22].

A distinction can be made between transient cavitation, involving a violent collapse of a bubble, and stable cavitation, which involves more gentle radial oscillations [15]. Typically, transient cavitation is involved in sonochemistry (chemistry induced by sonication) [23–25] and surface modifications (cleaning, erosion) [26], whereas stable cavitation can lead to local enhancement of streaming and mixing [27,28].

It is also known that transient cavitating bubbles can emit light (*sonoluminescence*, SL) [29–32]. For SL to occur, the pressure and temperature conditions inside the collapsing bubble have to satisfy the conditions for ionization and subsequent light emission [33]. $OH^{\cdot}$ radicals are formed when the conditions inside a bubble allow for the dissociation of water molecules (with dissociation energy $\Delta H = -5.1$ eV):

$$H_2O \overset{\Delta H=-5.1\ \text{eV}}{\rightarrow} OH^{\cdot} + H^{\cdot} \quad (2)$$

Some chemiluminescents react with $OH^{\cdot}$ radicals and produce light emission, a process known as *sonochemiluminescence* (SCL) [34,35]. Cavitating bubbles can generate SL or SCL, or both [36]; the population of SL and SCL active bubbles are not exactly the same and can strongly overlap [37–39]. The light emissions are generally faint, although SCL signals can be several orders of magnitude more intense than SL [37]. Dark conditions and the use of sensitive photo-multipliers are needed in order to detect SL or SCL, which then provide a measure of the amount of SL or SCL producing cavitation bubbles. Long exposure photography can be used as well, to obtain information on the spatial distribution of cavitating bubbles that produce SCL [40]. Temporal information on the cavitating bubbles can be obtained e.g. with a passive acoustic detector [41,42], however here we will use high-speed imaging [43], in order to obtain information on both spatial and temporal scales, and on the nature and onset of cavitation around the oscillating endodontic file.

The aims of this study were to quantify and to visualize the occurrence of cavitation around endodontic files. Using sensitive sonochemical methods for detecting SL and SCL, the occurrence of cavitation at various power settings is investigated, as well as the influence of the confinement of the root canal. Using a range of file types, the influence of different cross-sectional shapes, diameters and lengths of files on SL and SCL are studied. Measurements of the acoustic power density radiated by those files are provided by calorimetry. The SL and SCL measurements can provide information on the nature and characteristics of the bubbles. Long-exposure SCL photography and high-speed imaging provide additional visual support on the location and behavior of cavitating bubbles at different operation and confinement conditions.

2. Materials and methods

2.1. Ultrasound setup

A light-tight box with dimensions 1.2 × 1.0 × 0.5 m was constructed (see Fig. 1); dark conditions inside were verified by long-exposure photography. Inside the box, an endodontic file was positioned in a 1.0 × 1.0 × 4.0 cm cuvette (Plastibrand, Brand, Wertheim, Germany) or in a glass root canal (RC) model of bovine or human dimensions, manufactured in-house. The models were submerged and fixed inside the cuvette. The bovine-sized model was a cylindrical closed-end tube of diameter 2.3 mm and a length of 29 mm. The human-sized model was a cone of apical diameter 0.3 mm, a taper of 6% and a length of 20 mm. The two root canal models allowed for the investigation of the influence of confinement on the occurrence of cavitation. The light transmission coefficient through these glass models was measured and corrected for.

Fig. 2 shows a picture of an endodontic file and the different cross-sections; Table 1 gives an overview of the various files that have been tested. The first number in the name of the file indicates the diameter (×10 μm), the second number indicates the length (in mm). The K-files (Satelec Acteon, Merignac, France) have a square cross-section and are twisted along the length of the file, leading to rotation of the cross-section; the orientation of the cross-section at the tip of the file varies. The IrriSafe (IS) files (Satelec Acteon) also have a square cross-section but with rounded edges (with a radius of curvature of approximately 0.25× file radius); the ET25L (Satelec Acteon) has a circular cross-section [44]. One K-file (K15/25) was polished by the manufacturer to the same cross-section as IrriSafe files, in order to compare directly the influence of cross-section.

All files were driven with a commercially available endodontic ultrasound device (P-Max, Satelec Acteon, Merignac, France). The power settings on that device range (from low to high) from 'Green' via 'Yellow' and 'Blue' to 'Red', each with 10 steps. A previous study showed that the oscillation amplitude increased with power settings, with overlap between '10' and '1' in consecutive power color settings [14]. In the sonochemical experiments, the power setting was either increased (three measurements) or decreased (three measurements) between consecutive experiments, in order to investigate the presence of hysteresis. Each measurement group was measured three times; for each measurement a new file and fresh irrigant were used. Files that were suspected to have fractured (apparent from a sudden drop in SL/SCL signal) were also replaced.

The ultrasound device was switched on and off in cycles with a period of 10 s, consisting of 3 s ON and 7 s OFF (duty cycle of 30%). The rest phase in between pulses allows the fluid to return to its initial state with respect to its temperature and gas content. These pulses were generated with a pulse-delay generator (TGP110, TTi, Huntingdon, UK).

2.2. Sonoluminescence and Sonochemiluminescence

For measurements of the sonoluminescence (SL), the cuvette and root canal models were filled with MilliQ air–saturated water. A photomultiplier tube (PMT; R508, Hamamatsu Photonics, Hamamatsu, Japan) was placed next to the cuvette. The PMT received an electrical voltage of 1.6 kV from a DC power supply (6516A, Hewlett–Packard, Palo Alto, CA, USA). The PMT output was recorded at a rate of 300 kHz with a high-speed data acquisition device (DAQ; USB-6356, National Instruments, Austin, TX, USA), which was also recording the pulse signal. Calibration showed a linear response of the PMT up to an output voltage of 1 V, above which saturation occurs. Typical pulse and PMT signals are shown in Fig. 1c. The PMT signal was filtered with a running average with Gaussian weighing over 11 samples; the average value during each pulse was used as final SL or SCL value.

For sonochemiluminescence (SCL), air–saturated aqueous luminol (0.1 mM luminol in 0.1 M NaOH [both Merck, Whitehouse Station, NJ, USA]) solution was used, of which more details can be found elsewhere [37]. The SCL signal was measured using the same PMT equipment as for SL. Simultaneously, photos near the file were taken with a CMOS photocamera (D300, Nikon, Tokyo, Japan) and 50 mm, f/1.8 lens (Nikon) with an aperture of 1.8. The camera

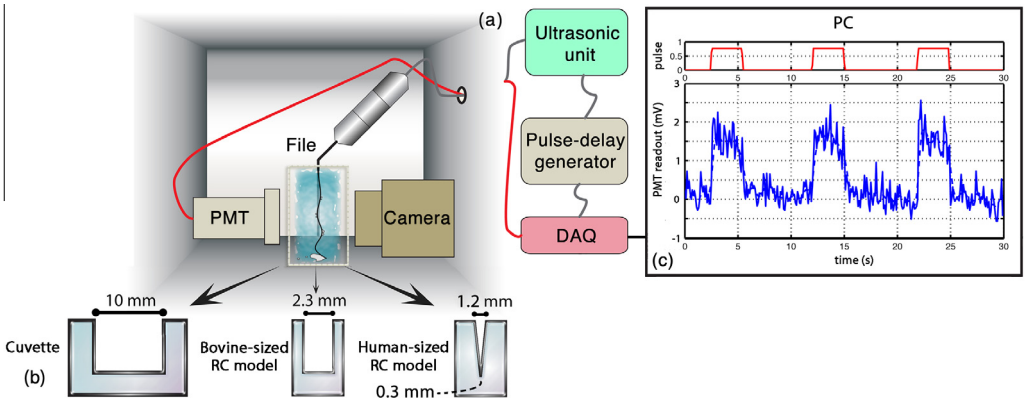

Fig. 1. Sketch of the experimental setup, not to scale. The light-tight box and the equipment it contains is depicted on the left (a), with the models sketched below (b). An example of the SL signal recorded on the PC is shown on the right (c).

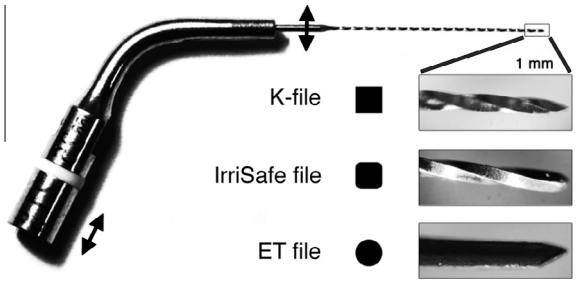

Fig. 2. Photo of an endodontic file and sketches of the three different cross-sections. The vibration direction is indicated with arrows.

exposure was set at 30 s, with highest ISO value (Hi1.0) and automatic white balance. A photo was taken in ambient light before the SCL photos were taken, to identify the location of the cuvette or root canal model walls. The sum of the pixel intensity value in a region-of-interest was calculated from the blue channel of the RGB photos, for a quantitative analysis of the luminol photos. The intensity of the blue channel along two files was correlated with the oscillation amplitude pattern of those files, following a previously described and validated one-dimensional model for endodontic files oscillating in air [44].

The reliability of the PMT measurements was tested using an interclass correlation coefficient among three measurements of SCL of an ET25L file in three consecutive days. Each measurement was repeated six times. A coefficient score of 0.994 for single measurements with $p < 0.001$ was found, assuring a high reliability and repeatability.

The chemical activity of the $OH^{\cdot}$ radicals produced by transient cavitation was compared to those dissolved in a NaOCl solution by a fast injection of luminol into the cuvette, filled with a 10% NaOCl solution (Sodium Hypochlorite, Sigma–Aldrich, St. Louis, MO, USA). The PMT response was recorded using the equipment described above. The luminol was injected at a flow rate of 1 mL/min through a 27G needle, driven by a syringe pump (NE1010, New Era Pump Systems, Wantagh, NY, USA).

2.3. Statistical analysis

Students *t*-tests for independent samples were performed to assess differences in SCL between files with different lengths (21 vs. 25 mm) and cross-sections (square (K) vs. square with round edges (IrriSafe) vs. circular (ET)). ANOVA tests were used to assess the influence of diameter (size 10 vs. 25 vs. 30) in SCL and of the confinement (cuvette vs. bovine-sized RC model vs. human-sized RC model) in SL. For all tests, *p*-values <0.05 were considered statistically significant.

2.4. Calorimetry

The acoustic power density radiated by three files was measured inside the cuvette and the two root canal models using calorimetry. A 0.2 mm diameter T-type thermocouple with digital

Table 1
Overview of the file types and measurements on them. Files that allow for comparison of file length (*L*, solid line), diameter (*D*, dashed line) or cross-section (*CS*, double line) are linked with lines. * Polished to the same cross-sectional shape as the IrriSafe files.

File type	K10/21	K10/25	K15/25	K15/25P*	K25/21	K30/21	IS25/21	IS25/25	ET25L
Cross-sectional shape	□	□	□	▢	□	□	▢	▢	○
Sonochemoluminescence									
Cuvette	×	×	×	×	×	×	×	×	×
Sonoluminescence									
Cuvette	×	×	-	-	×	-	×	×	-
Bovine-sized RC model	-	-	-	-	×	-	×	×	-
Human-sized RC model	-	-	-	-	×	-	×	×	-
Calorimetry									
Cuvette	×	×	×	×	×	×	×	×	×
Bovine-sized RC model	-	-	-	-	×	-	×	×	-
Human-sized RC model	-	-	-	-	×	-	×	×	-

L D CS D CS L CS D

read-out (HI 93552R; HANNA Instruments, Woonsocket, RI, USA) was fixed inside the cuvette. In the case of the root canal models, the thermocouple was glued inside a side channel of diameter 1.5 mm located at 2 mm from the apex of the root canal. Sampling was performed every 2 s with an accuracy of 0.1 K.

The files were driven for 1 min by the same endodontic device at power setting 'Blue 1' or 'Red 10'. The acoustic power density W_{ac} (in W/L) was determined from the temperature increase ΔT measured during a time interval Δt:

$$W_{ac} = \frac{\rho c_p \Delta T}{\Delta t} \quad (3)$$

with ρ the density of the liquid and c_p its specific heat.

2.5. High-speed visualization

The generation of cavitation bubbles on the files was visualized using a high-speed camera (HPV-1, Shimadzu Corp., Kyoto, Japan), recording at a frame rate of 1 million frames per second. The camera was attached to a microscope (BX-FM, Olympus, Tokyo, Japan) providing 20× magnification, resulting in a resolution of 3 μm/pixel. Illumination was provided in bright-field mode using a continuous wave light source (ILP-1, Olympus). The file of interest was positioned parallel or perpendicular to the image plane, such that a side-view of (a section of) the file or its cross-section was visible and in focus. The file itself was submerged in a large water tank (75 × 62 × 117 mm) filled with tapwater. For one set of experiments, degassed water, luminol or NaOCl (10%, Sigma–Aldrich, St. Louis, MO, USA) was used instead of tapwater.

The files were driven at power settings 'Blue 5' or 'Red 5' using the endodontic ultrasound device.

In one additional experiment a dentin disc was placed at a distance of approximately 200 μm from a K15/25 file, in order to investigate the influence of a neighboring wall on the cavitation phenomenon. The dentin discs (diameter 5 mm, thickness 1.5 mm) were prepared from freshly prepared bovine incisors using a trephine [45].

3. Results

3.1. Sonochemical characterization

3.1.1. SL measurements

During each pulse of ultrasound (3 s), there was an increase in PMT signal for the SL measurements, rising within 1 s, and falling off to the noise level within 1 s after the pulse ended (see Fig. 1c for an example). As a general trend, the higher the ultrasonic power setting, the higher the signal output of the PMT. Below a power setting of 'Blue 1' no increase in PMT signal above the noise level could be detected.

The SL signal for one example file (IS25/21) inside the cuvette and bovine- and human-sized root canal models is plotted in Fig. 3, showing that a smaller confinement increases the SL signal. This trend was observed for all files ($p < 0.001$).

3.1.2. SCL measurements

The signal for SCL during each pulse was similar in shape to that of SL, but approximately 3 orders of magnitude higher. Therefore, already at the low power setting of 'Green 5' (below the power settings plotted in Figs. 3 and 4) a SCL signal could be observed for several files. The SCL signal is plotted in Fig. 4 as a function of power setting for various files oscillating inside the cuvette. The average and standard deviation of the 18 measurements are used. For all files there was an increase in SCL signal for increasing power setting. The SCL signal ranged over 5 decades and was found to be highly dependent on the file type. Both IrriSafe files resulted in a

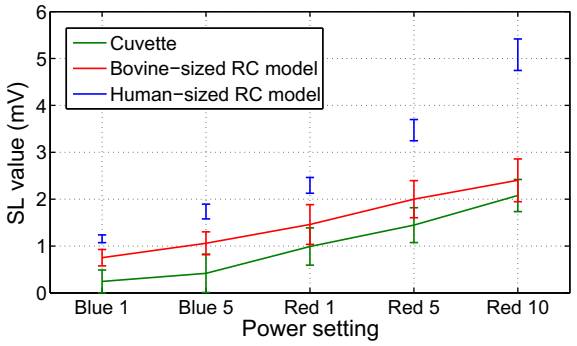

Fig. 3. Average and standard deviation of the SL signal for an IS25/21 file inside different confinements (colors). (For interpretation of the references to colour in this figure legend, the reader is referred to the web version of this article.)

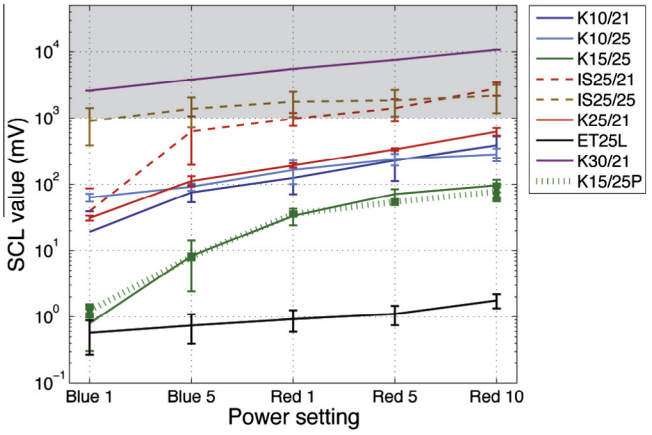

Fig. 4. Average and standard deviation of the SCL signal measured with the PMT for nine different files, with varying length, diameter and cross-section, oscillating inside the cuvette. The shaded area above 1 V represents saturated PMT response and therefore underestimated results. (For interpretation of the references to colour in this figure legend, the reader is referred to the web version of this article.)

SCL value higher than the K-files of similar dimensions ($p = 0.001$). Files with a larger diameter generally also resulted in a higher SCL values ($p < 0.001$). The ET25L, with a circular cross-section, resulted in significantly lower SCL values ($p < 0.001$). The polished K15/25 file showed no differences with the unpolished K15/25 file ($p = 0.567$).

There is no clear correlation between the amount of cavitation observed and the oscillation amplitude of the file tip as obtained

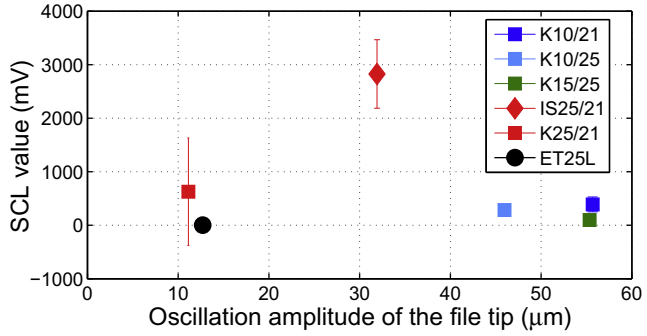

Fig. 5. Average and standard deviation of the SCL signal for six files, plotted versus its oscillation amplitude as determined in a previous study [44]. (For interpretation of the references to colour in this figure legend, the reader is referred to the web version of this article.)

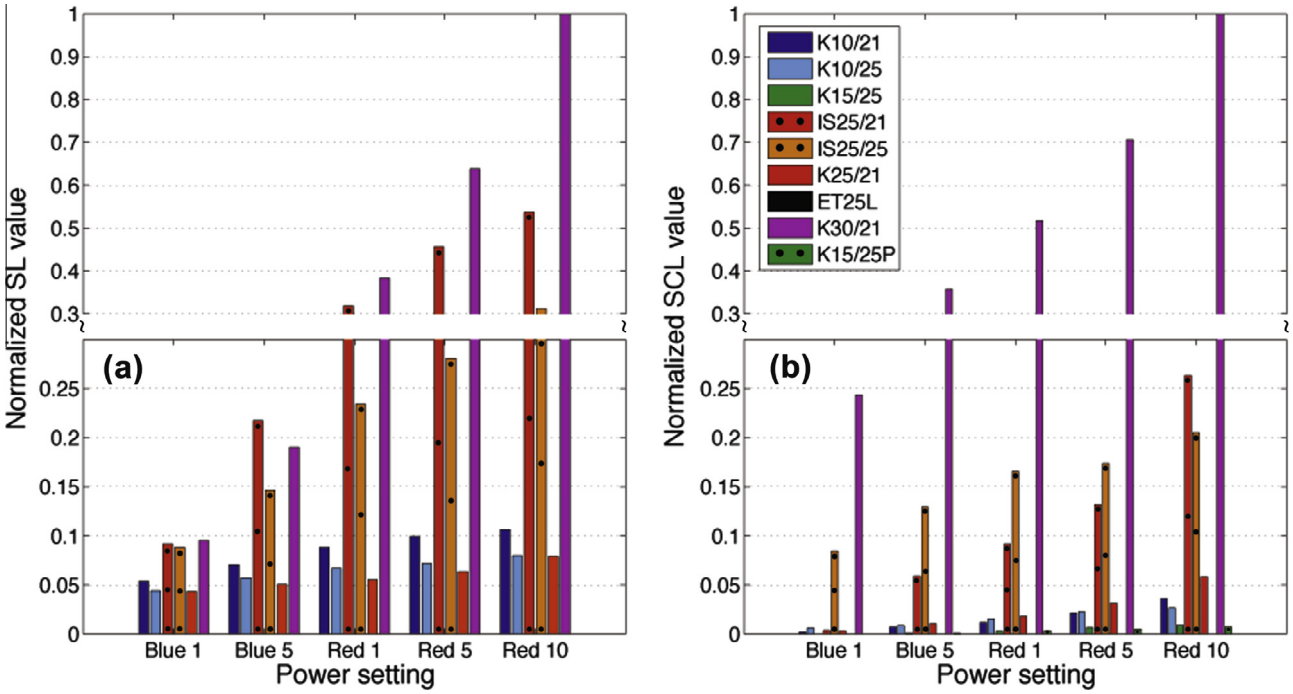

Fig. 6. SL (a) vs. SCL (b) for various files. Note the double *y*-axis scaling. (For interpretation of the references to colour in this figure legend, the reader is referred to the web version of this article.)

in a recent study [44], see Fig. 5. This suggests that not only the oscillation amplitude (as a function of power) but also the file diameter and cross-section have an influence on the generation of cavitation. Further discussion is provided in the remainder of this work.

The injection of luminol into a NaOCl solution showed a rapid increase of the SCL signal, rising within one second to a value of 60 V, where the PMT is fully saturated.

3.1.3. Comparison of SL and SCL measurements

In Fig. 6 the SL and SCL results for all files have been normalized to the maximum value of the K30/21 file. Both methods show that the K30/21 file generates the highest amount of cavitation, followed by the two IrriSafe files. For SL, the ratio between files is different than for SCL, which can be attributed to the generation of bubbles that are either more light-producing or more chemically active [37,38,46]. Also, for SCL of several files the PMT signal was easily saturated, affecting the relative amplitudes, although the ordinal scale should not be affected. The increase in cavitation with increasing power setting is also apparent from these plots.

The differences in SL and SCL values between increasing and decreasing the power setting for consecutive experiments were not significant. Therefore hysteresis was ruled out, justifying the combination of the data. Also, it can be concluded that the possible changes in temperature and gas content were not enough to alter the overall cavitation features.

3.1.4. Luminol photography

Overlaying the long-exposure photos with those of the confinement showed a blue area (luminol) between the file and the wall (see Fig. 7), especially at the higher power settings. In the cuvette there is a large area of luminol photo signal along the file, with brighter areas along the file that can be related to a distribution of nodes and antinodes along the file, see Fig. 8. The bright areas are separated by a few millimeters, which is consistent with the distance between the antinodes on an oscillating file in air. The locations of the maximum intensity in the luminol photos and those of the oscillation patterns do not match exactly, because the oscillation patterns are obtained from a simulation for files oscillating in air [44]; in water or luminol, the wavelength will increase, which will result in a better match of the maxima in the luminol photo intensity with the antinodes. Nevertheless, the areas of higher luminol photo intensity can be associated with the location of the antinodes away from the tip of the file and not with the

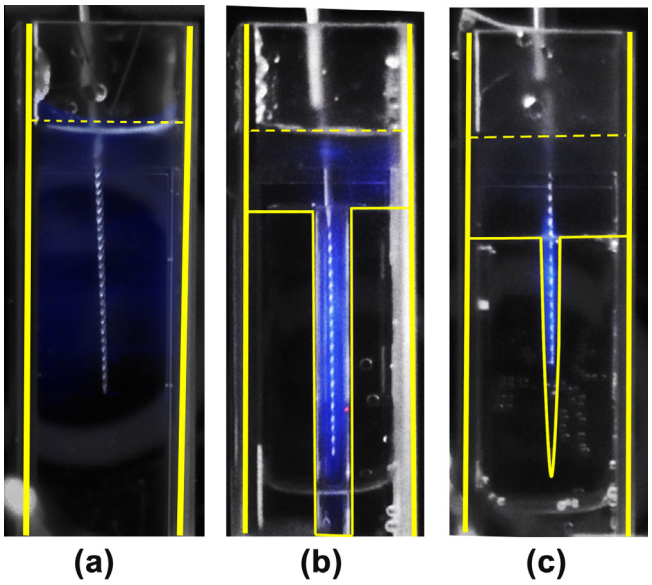

Fig. 7. Overlay of luminol photos (blue) with ambient light photos, showing the spatial distribution of luminol inside the cuvette (a) and bovine-sized (b) and human-sized (c) root canal models. The confinements have been outlined with solid yellow lines; the luminol-air interface is indicated with a dashed yellow line. The white bar in (a) is 2.5 mm wide. (For interpretation of the references to colour in this figure legend, the reader is referred to the web version of this article.)

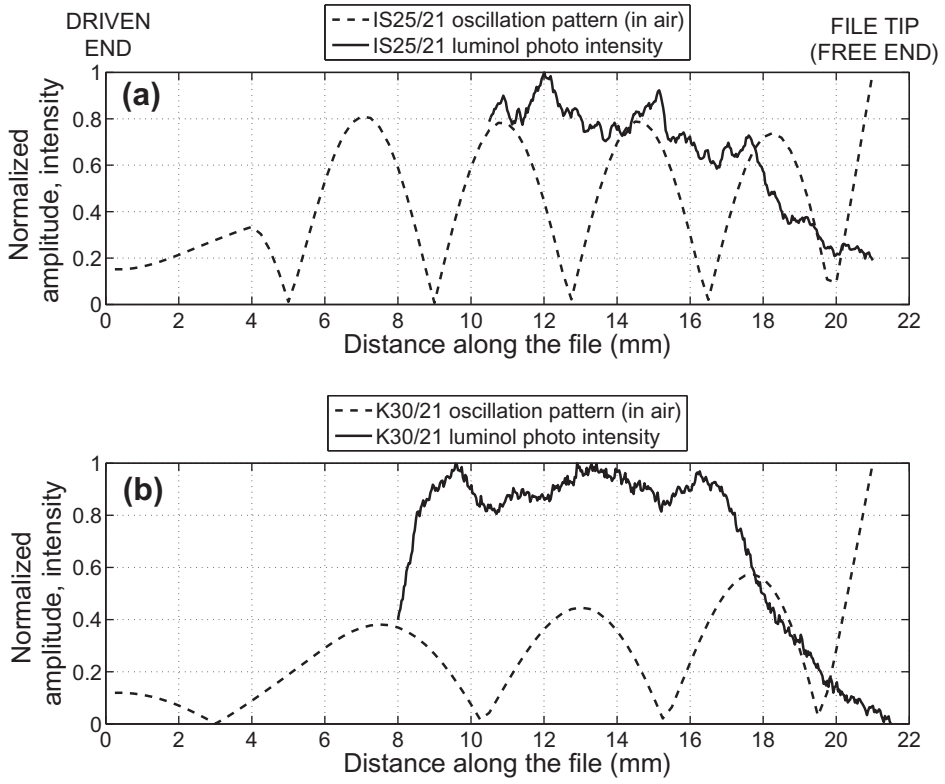

Fig. 8. Comparison of the normalized intensity in the luminol photos of two files with the oscillation characteristics of those files. The oscillation characteristics are obtained from a previously described simulation [44] of the files oscillating in air. In water, the wavelength has been reported to increase, which will improve the match of the maxima in the luminol photo intensity with the antinodes.

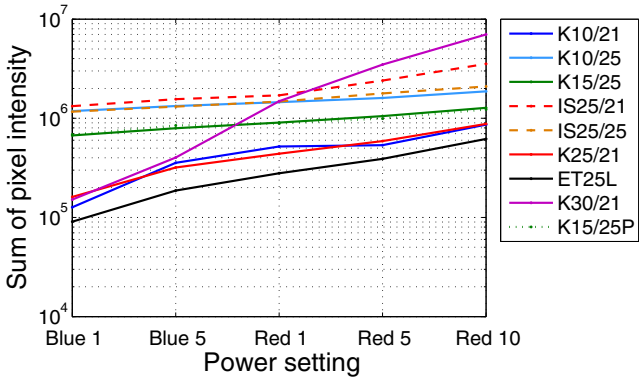

Fig. 9. Luminol intensity for 5 power settings and 9 files, to be compared to Fig. 4. The photo intensity ranges only three decades, whereas the PMT signal spanned 6 decades. (For interpretation of the references to colour in this figure legend, the reader is referred to the web version of this article.)

tip of the file itself. Toward and beyond the tip of the file, the luminol photo intensity decreases.

In the confinement of the bovine-sized and human-sized root canal models, the luminol photo intensity was observed to be uniformly distributed between the file and the wall. The luminol photo signal was also observed beyond the file tip toward the apex of the confinement.

A quantitative analysis of the luminol photos showed an increase of intensity with increasing power (Fig. 9). These trends were similar to the SL and SCL results (Fig. 4). However, the luminol photos have a resolution of 2 decades whereas the SCL data spanned more than 5 decades, making the SL and SCL methods more sensitive than the luminol photography method.

3.1.5. Calorimetry

Sonication of the water inside the cuvette showed a linear increase in temperature within the measurement time of 1 min, see Fig. 10a. The IS25/25 file driven at the high power setting was found to have the highest slope (0.08 K/s) and a maximum temperature increase of 4.9 K, with the slope and temperature increase at low power setting being approximately half of those values. The K25/21 and IS25/21 file at high power both had a slope of 0.02 K/s.

Inside the bovine- and human-sized root canal models (Fig. 10b and c, respectively), the temperature increased by 12 and 14 K, respectively, within 1 min. The slopes were not linear but showed an initial fast rise in temperature, followed by a more gradual increase. This change in slope could be due to heat conduction by the glass confinements that starts to play a role after a few seconds.

Table 2 shows the acoustic power density as calculated from Fig. 10a-c and Eq. (3), assuming a linear temperature increase over time. The acoustic power density is on the order of 0.1–1 W/L. The confinement of the bovine-sized root canal model increased the acoustic power density by a factor of 2.5 to 6, depending on the file. An even smaller confinement, of the size of a human root canal, increased the acoustic power density by another factor of 1.2–2.8. In all confinements, the IS25/25 file had the highest acoustic power density, followed by the K25/21 and IS25/21 files.

3.2. High-speed visualization

High-speed recordings confirmed of the occurrence of cavitation, predominantly at the tip of the file where a large cloud of bubbles was formed with a size on the order of the file diameter. At subsequent antinodes along the file, single, smaller cavitation bubbles were observed with diameter on the order of 10 μm, see

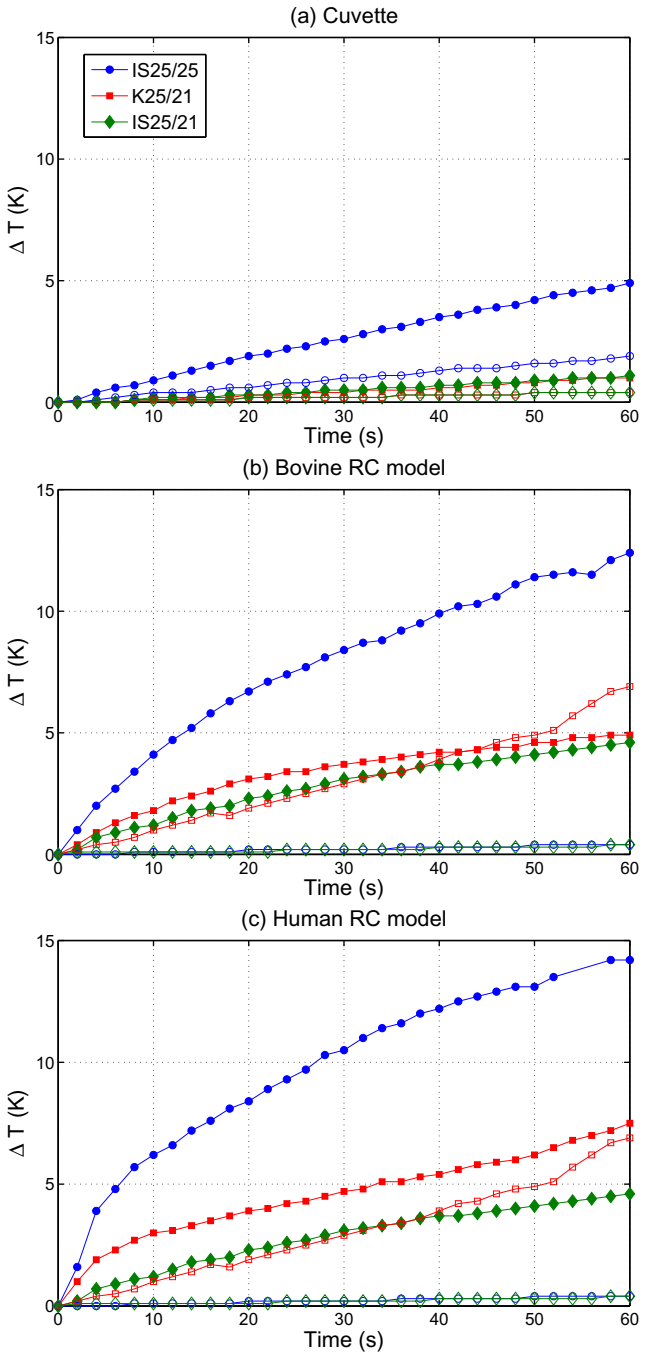

Fig. 10. Plot of temperature increase versus ultrasound sonication time, for three files (colors), inside the cuvette (a) or bovine-sized (b) or human-sized (c) root canal (RC) model. Low and high power are indicated with open and closed symbols, respectively. The values are averages of 3 measurements. The standard deviations are not indicated for clarity but are at most 1 K. (For interpretation of the references to colour in this figure legend, the reader is referred to the web version of this article.)

Table 2
Acoustic power density (W/L) for three different files and three confinements calculated using Eq. (3). The files were driven at power setting 'Red 10'. The standard deviation is 0.07 W/L.

W_{ac} (W/L)	IS25/25	K25/21	IS25/21
Cuvette	0.34	0.07	0.08
Bovine-sized RC model	0.86	0.32	0.48
Human-sized RC model	0.99	0.86	1.35

Fig. 11 and Supplementary Movie 1. The generation of the large bubble cloud at the tip of the file can be observed in more detail in the recordings of the cross-section of the file, see Fig. 12 and Supplementary Movie 2.

The orientation of the square cross-section was observed to have a large influence on the cavitation formed at the file edges. When the in-focus tip of the file oscillated along the diagonal of the cross-section ('diamond'), cavitation was observed at the corners of the cross-section. However, when the in-focus tip of the file had one of its sides in the direction of oscillation ('square'), the cavitation cloud was observed to form out-of-focus, i.e. at a part of the file with diamond orientation. The distance between square and diamond orientation in the axial direction along the file is 0.25 mm [44], whereas the focal depth of the microscope optics is around 0.10 mm.

The bubble cloud was observed to grow in front of the moving file already during the deceleration of the file, i.e. before reaching its maximum displacement. This can be attributed to a phase difference between the file oscillation velocity and the induced pressure, as predicted in another study [22].

The bubble cloud was observed to grow and to collapse twice per period in the wake of the oscillating file. Small bubbles with a diameter less than 5 μm were observed to split off from the bubble cloud and to obtain a steady velocity of approximately 1 m/s away from the file. These bubbles could be observed for at least 3 ms before dissolving or moving out of focus. The generated bubbles were therefore likely to be of the stable cavitation type. This was further confirmed by their tendency to flow along a glass wall placed nearby rather than collapse onto it.

Degassing the tap water before oscillating the file resulted in a reduction (to almost zero) in the size of the bubble cloud and the number of bubbles split off (see Fig. 13). This behavior is expected since there is less gas and less nuclei available to nucleate bubbles. Oscillating the file in a luminol solution appears not to affect the

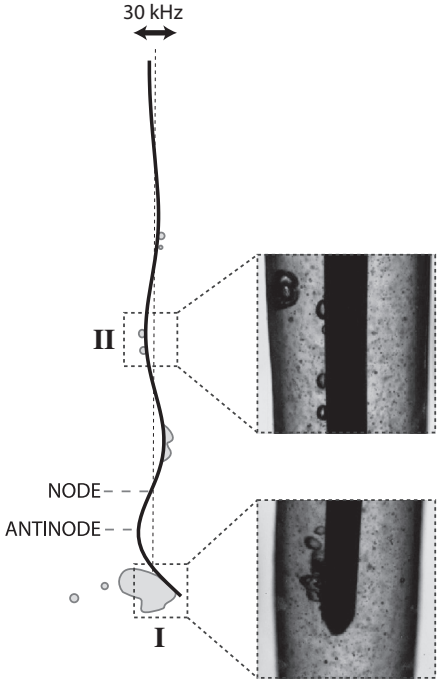

Fig. 11. Sketch of the occurrence of cavitation along the length of an oscillating file, based on Supplementary Movie 1. At the tip of the file (I), a large cavitation bubble cloud is formed; at other antinodes (II), only small, single bubbles are observed. Still images are taken from Supplementary Movie 1, where the file is oscillating inside the confinement of a root canal model.

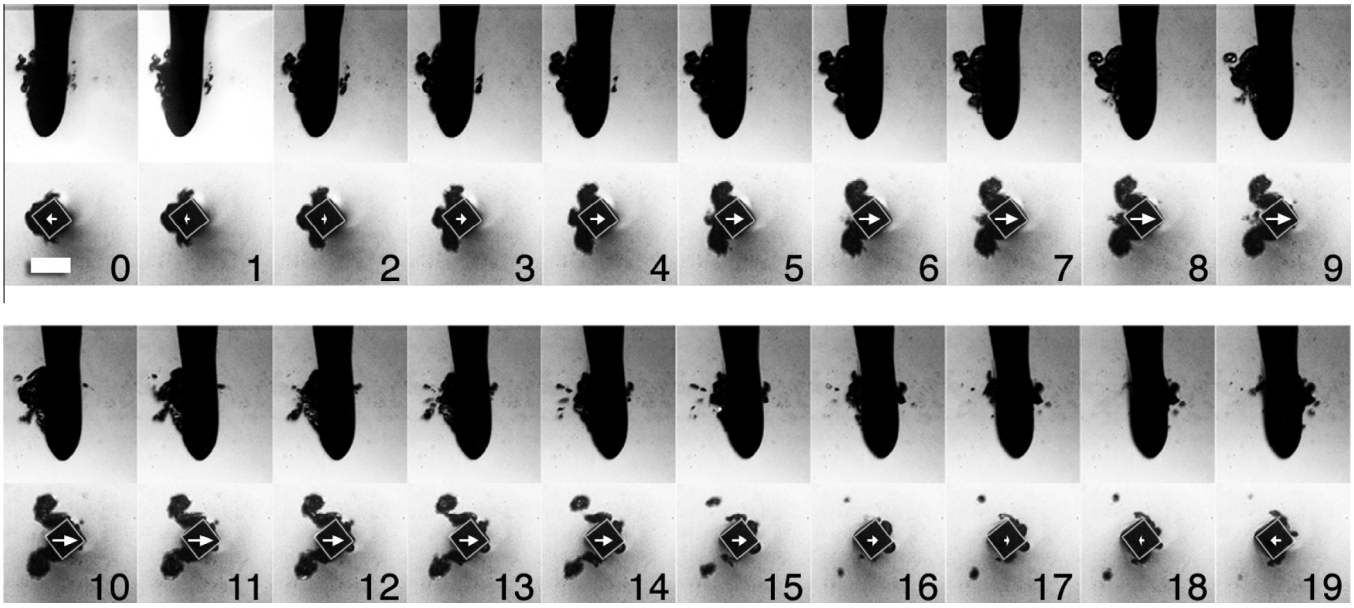

Fig. 12. Cavitation at the tip as visualized from the side (upper rows) and head-on (lower rows), during one half of an oscillation cycle. The white arrows indicate the direction in which the file moves; their length represents velocity magnitude. The numbers indicate time in microseconds. The white bar is 200 μm. See also Supplementary Movie 2 for the cross-sectional view.

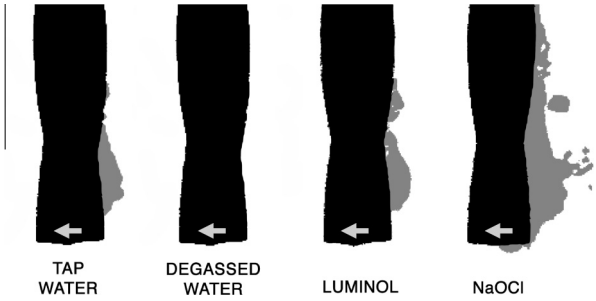

Fig. 13. Representative images of the cavitation cloud (grey) on the tip of a K-file (black), in different liquids. The arrows indicate that the motion of the file is to the left. The diameter of the file at the tip is 150 μm.

size of the bubble cloud compared to tap water. When using a NaOCl solution, on the other hand, a large increase in size of the bubble cloud was observed. It also resulted in larger bubbles being shed off, which is a typical effect of a salty solution that is described in literature [47,48].

A dentine wall placed within 200 μm of the oscillating file did not reduce or increase the amount of cavitation occurring close to the file, see Fig. 14. However, more interesting was the observation that the bubble cloud tended to collapse onto the file rather than onto the wall, independent of the distance between the file and the wall. Cavitating bubbles were only incidentally observed on the dentine wall. Similar observations were made for the file oscillating inside the confinement of the root canal (see Supplementary Movie 1), where cavitation on the glass wall was only observed in a limited number of cases. However, the roughness of the wall of a real root canal is much larger than that of the glass models employed here, which increases the number of potential bubble nucleation sites. More cavitation may therefore be expected inside a real tooth.

The water–air interface at the coronal part of the root canal was observed to be unstable when certain files and insertion depths were used, see Fig. 15 and Supplementary Movie 3. This instability can be related to an antinode of the oscillating file coinciding with the air–water interface. Droplets were observed to split off from the unstable interface, leading to a reduction of the amount of fluid present in the root canal, as also reported in a previous study [3]. The instability of the interface also led to air entrainment, resulting in large and stable bubbles (more than 100 μm in diameter) in the root canal liquid volume. Such stable bubbles could oscillate together with the ultrasonic file and exhibit surface oscillations. This can locally increase the streaming significantly, even at remote locations such as inside a side channel of the root canal (see Supplementary Movie 4).

4. Discussion

The sonochemical dosimetry and the visualization measurements have shown that cavitation can take place around endodontic files, even within the confinement of a root canal model. The amount of cavitation varied between the file types but always increased with increasing power setting. The observation that cavitation could already be measured for very low power setting (Green 5), where the oscillation velocity of the file is below the 15 m/s cavitation threshold limit as derived before, suggests that the fluid

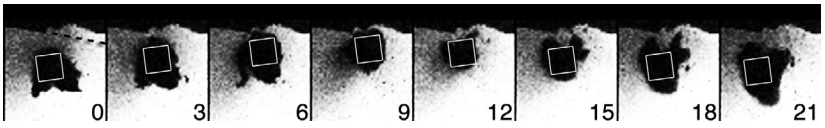

Fig. 14. File next to a dentin wall, showing no collapse of the bubble cloud on the wall. The dashed line in the first panel indicates the original location of the wall, showing the damage done by the file itself. The numbers indicate time in microseconds; the white bar is 200 μm.

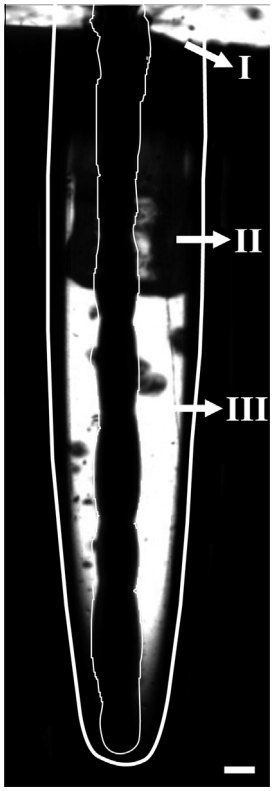

Fig. 15. Air entrainment due to an oscillating file (outlined in white) inside a glass root canal model (thick white line). An antinode of the oscillating file leads to instabilities at the air–irrigant interface (I), resulting in the generation of a spray of droplets of irrigant. After some time, this loss of irrigant results in a large volume fraction of the root canal being occupied by air rather than irrigant (II). Stable bubbles can split off from this air pocket (III). The white bar is 200 μm.

flows around the edges of the file with a velocity higher than the oscillation velocity of the file. This phenomena is known as *edge cavitation*.

Regarding the geometrical properties of the file (length, diameter and cross-section) we observed an increase in the SL and SCL signals with increasing file diameter, which can be explained by a larger amount of fluid that has to be displaced by a thicker file, leading to larger velocity and pressure gradients. The polishing of the square cross-section of the IrriSafe files did not affect the SL and SCL signals.

Changing the file length, diameter or cross-section of the file was shown previously to have a large and not straightforward influence on the file oscillation characteristics [44]. However, no clear relation between SCL value and the predicted oscillation amplitude at the tip of the various files was found (Fig. 5), in spite of our findings reported here and that of a previous study [12] that a higher amplitude (power setting) for a single file does increase the SCL value. This leads to the hypothesis that the cavitation cloud observed at the tip of the file does not induce a measurable amount of SCL, but that it is rather the smaller bubbles that were observed at the other antinodes that contribute to the SCL emission. This hypothesis is supported by the observation that the IrriSafe files generated a higher SCL signal. The IrriSafe files have a lower tip oscillation amplitude than K-files of similar dimension, but all antinodes on the IrriSafe files have approximately the same amplitude due to the absence of a taper on these files [44], leading to a preference for more and smaller bubbles all along the file rather than a large bubble cloud at the tip. The K-files typically have a high amplitude at the tip, leading to the formation of the cavitation bubble cloud, but the amplitude of consecutive antinodes decreases rapidly and seems not to generate any cavitation. The luminol photos (as well as additional visualizations not included here) also support this hypothesis, as generally near the tip of the files the intensity in the long-exposure photos decreased. It should also be considered that there may be bubbles present with a size smaller than the optical resolution, which nevertheless could contribute to the SL and SCL signals.

The different nature of the large bubble cloud and the small individual bubbles can be explained in the following way. Bubble clouds as the one observed at the file tip can cause acoustic shielding, which reduces the ultrasound intensity that is experienced by bubbles inside the cloud. As a consequence, the energy focusing effect of each individual bubble collapse and the active bubble population are reduced, leading to less SCL intensity when compared to the single bubbles induced at locations along the file with lower amplitude [49,50]. It is expected that these spherical bubbles collapse more symmetrically and efficiently and are therefore contributing the most to radical production. Cavitating bubbles in bubble clouds furthermore have a smaller expansion maximum radius [51], which also affects the SL and SCL [50].

Considering the file oscillation amplitude in terms of acoustic power, similar results are reported in the literature. It has been found that higher power can be detrimental to $OH^{\cdot}$ radical formation [25,37]. The reason for this is that a population of smaller and more spherical bubbles is proportionally larger at low power, as the growing and collapsing bubbles do not affect each other, contrary to bubble formation at a high power setting. Furthermore, numerical simulations of $OH^{\cdot}$ production rates suggest that a decrease of SCL takes place if the bubble temperature inside an air bubble is too high due to a high pressure. $OH^{\wedge}$. radicals are then consumed by oxidizing nitrogen inside the bubble [52]. The bubble temperature can also increase as a result of bubble–bubble interaction with smaller bubbles [53].

As mentioned in the Introduction, cavitating bubbles can generate SL or SCL, or both; the population of SL and SCL active bubbles are not exactly the same and strongly overlap [37–39]. In this study we have localized and identified the bubbles that are SCL-active using both high-speed imaging and long-exposure luminol photography. Additional experiments using long-exposure SL photography equipment, as reported elsewhere [37,54], will have to be performed to provide similar evidence for the situation of SL emission.

The calorimetry measurements have shown that during one minute, the temperature of the liquid increases with 1–15 °C (Fig. 10). According to literature [55], a drastic decrease in SL in water takes place as temperature increases from 15 to 70 °C. As the temperature increases in the liquid, the gas concentration decreases, making the number of nucleated bubbles decrease. Also the ratio of vapor to gas increases as the solubility of gas decreases, which diminishes SL. Furthermore, the bubble can become saturated by vapor and, in the final stage of the adiabatical collapse, can arrest the compression phase, decreasing the SL intensity. There are several other parameters and reactions taking place inside the bubble (which depend on frequency as well) that are beyond the scope of this study but are reported elsewhere [52,55–58]. In this study, however, the ultrasound is pulsed with 3-s pulses and 7-s rest intervals, thereby limiting such temperature effects. Pulsation is furthermore reported to have beneficial sonochemical effects, for example when the pulse length is tuned to the dissolution time of the generated bubbles [59].

The reaction between NaOCl and luminol resulted in a SCL value that was much higher than the highest value of SCL produced for all of the files. As saturation of the PMT was likely, the ratio of $OH^{\cdot}$ production by cavitation to that dissolved in the NaOCl solution could not be determined. Nevertheless the enhancement by

$OH^{\cdot}$ production by cavitation to the chemical cleaning effect of NaOCl is likely to be small.

The observation that the areas of high intensity in the luminol photos are not limited to the vicinity of the file but are actually spread out between the file and the wall, suggests that the reaction between the luminol and the radicals produced by cavitation does not always take place in the vicinity of the file. Cavitation can also take place at crevices in the circumferential wall and tiny bubbles that have split off from the bubble cloud (possibly smaller than the optical resolution of 3 μm/pixel). These phenomena have been observed and modeled before [60]. Within the confinement of the root canal the acoustic field may be such that cavitation of small bubbles can occur even beyond the file tip. These small bubbles do not loose their sphericity and are therefore very SCL active compared to the larger bubbles.

A smaller confinement was found to lead to an increase in the SL and SCL signals. This could be attributed to the increase in acoustic power density emitted within these confined geometries, due to the presence of the root canal walls [61]. It could also be attributed to the increase in pressures as predicted in a previous study [22]. It should be noted that the human-sized root canal models have a conical shape as opposed to cylindrical, which could affect the SL and SCL signals because of the decreasing space around the file toward its tip. It should also be noted that the cuvette may not be considered an 'unconfined' case, as the sides of the cuvette are 50 times larger than the typical diameter of a file.

In the present study, the files were positioned in the center of the root canal during the sonochemical characterization experiments, which, however, is difficult inside the small human-sized root canal model. A recent study [62] has indicated that, during clinical use of Ultrasonically Activated Irrigation, contact with a wall cannot be avoided, which introduces a secondary, audible frequency on top of the 30 kHz oscillation. These two frequencies can lead to constructive or destructive interference, resulting in occasionally higher or lower velocities, with an associated probability of cavitation occurrence (see Supplementary Movie 5).

The bubble cloud at the file tip tended to collapse onto the file itself, not on a nearby wall, where removal of biofilms and smear layer is required. Erosion and cleaning of a hard wall takes place by jetting of collapsing bubbles and shock waves induced upon collapse [63,64,26]. However, bubbles collapsing near a soft wall may generate a jet away from the wall, thereby pulling the soft material off the wall [65]. Therefore if the file is close to the wall when the bubble collapses, this cavitation cloud may enhance the cleaning of root canals, without causing erosion damage to the dentin wall.

The reported observation during clinical use of UAI that aerosols are generated outside of the root canal cavity [66], suggests that instability of the irrigant–air interface and resulting air entrainment as shown here, does indeed take place. Air entrainment was also often observed for the glass models employed in this study when not submerged in the cuvette, leading to a root canal filled with large air bubbles ($\mathcal{O}$(100 μm) in radius). Air entrainment results in loss of irrigant, in the extreme case preventing generation of acoustic streaming [22], for which a fluid is required. The entrained bubbles, however, could enhance the cleaning of the root canal system by locally increasing the streaming and mixing. In different studies it was furthermore reported that the increased uptake of gas by the liquid at higher powers resulted in an increased SL value [67]. The free surface oscillation itself has previously been reported to negatively affect SCL values [37,68].

The SL and SCL methods of cavitation detection used in this study were more sensitive than the method using the luminol photos (Fig. 9). Therefore, previous studies using luminol photography [7,13] probably underestimated the occurrence of cavitation, which is present already for lower power settings as this study shows. Nevertheless, the luminol photos are useful in obtaining information on the spatial distribution of cavitation (Fig. 8), which cannot be obtained from the SL and SCL PMT measurements. Other dosimetry methods have been reported in the literature, e.g. terephtalic acid (TA) ([69]). However, a pilot study showed that the concentration range that was generated with our ultrasound equipment was below the sensitivity level of the TA method. Another dosimetry method reported recently [70], using tert-butyl nitrite (t-BuONO), is a more promising method and has been proven to be applicable *ex vivo* up to the volume of bovine root canals. A comparison with the present methodology remains to be performed.

In future work, additional temporal detail and insight into the oscillatory or transient nature of the cavitation can be obtained using passive acoustic detection. The high-speed imaging performed in the present study provides additional information on the occurrence of cavitation in a small region-of-interest during a short time span. Additionally, the luminol photos show a large region-of-interest time-averaged over several seconds. The combination of these three techniques is then a good approach for an integral characterization of endodontic files and equipment. We have shown that such characterization of cavitation in Ultrasonically Activated Irrigation is relevant because cavitation occurs and may contribute to mechanical and chemical cleaning.

5. Conclusion

The generation of cavitation in different root canal models, generated by the oscillation of several endodontic files, was demonstrated even at low power settings by means of sonochemical (SL and SCL) and optical techniques. This methodology of testing endodontic devices was found to be sensitive and is a useful method in the characterization of existing or new endodontic files and devices.

The amount of cavitation varied between the files; the averaged SCL signals spanned 5 decades and increased with increasing power setting. Generally speaking, a larger diameter increased the cavitation activity. The confinement of a bovine and a human root canal was mimicked and showed an increase of cavitation activity by an increase in the number and size of the bubbles, and an increase in the SL and SCL values.

High-speed recordings showed that a cloud of cavitation bubbles, generated at the sharp edges of a file with a square cross-section, only collapsed on the file itself and not on a nearby wall. This bubble cloud did not contribute to SCL, but may help the root canal cleaning by pulling on material on a nearby wall. At antinodes with smaller amplitude, small individual bubbles were observed and they contribute for the major part to the SL and SCL observed.

Air entrainment at the liquid–air interface was found to lead to stable cavitation bubbles which promote streaming and mixing.

Acknowledgements

The authors thank Sib Jan Boorsma and Gert-Wim Bruggert for constructing the light-tight box and Cock Harteveld at COPS (University of Twente) for the loan of the PMT equipment. Furthermore we acknowledge Roy Kooijman of TCO (University of Twente) for manufacturing the glass root canal models, Michel Hoogenkamp at ACTA for the dentin discs, and Francis Dieras of Satelec Acteon and Olivier Breguet of FKG for polishing the files to the specific cross-section. B.V. and D.F.R. are financially supported by the Dutch Technology Foundation STW (projects 07498 and 07391, respectively).

Appendix A. Supplementary movies

A.1. Movie 1 – Cavitation along the file

Composition of 15 high-speed recordings of a file (oscillating shape in the center) oscillating inside a glass root canal model (walls). The sinusoidal oscillation amplitude pattern of the file can be seen. A cloud of cavitation bubbles can be observed at the tip of the file; smaller cavitation bubbles occur at other antinodes. Recording speed is 500 Kfps; the diameter of the file is 200 μm.

A.2. Movie 2 – Cavitation around a square cross-section

High-speed recording of the generation of a cavitation cloud around a file with a square cross-section, viewed toward the tip of the file. Recording speed is 1 Mfps; the cross-section has sides of 200 μm.

A.3. Movie 3 – Air entrainment

High-speed recording of the instability of the air–irrigant interface at the coronal opening of the root canal. Once the instability has developed, droplets can be observed to split off. After some time, the irrigant loss is significant, leading to air entrainment in the root canal. The final frame shows the state after 1 s. Recording speed is 10 Kfps; the file diameter is 200 μm.

A.4. Movie 4 – Stable bubble oscillations

Stable oscillations of a bubble trapped in a side channel. These bubbles were generated by air entrainment during a preceding experiment. The bubble oscillates optimally if its resonance frequency matches the frequency of the oscillating file, for which the bubble radius should be 100 μm. Recording speed is 10 Kfps, the file diameter is 200 μm.

A.5. Movie 5 – Contact with a wall

Oscillation of a file inside a cylindrical confinement, as viewed toward the tip. The file was put in contact with the wall on purpose, leading to a secondary frequency of the file oscillation. Beating of these two frequencies leads occasionally to a high velocity moving the file away from the wall, during which cavitation at the file tip can be observed. Recording speed is 125 Kfps; the diameter of the confinement is 600 μm.

References

[1] A.D. Walmsley, Applications of ultrasound in dentistry, Ultrasound in Medicine and Biology 14 (1) (1988) 7–14.
[2] L.W.M. Van der Sluis, M. Versluis, M.K. Wu, P.R. Wesselink, Passive ultrasonic irrigation of the root canal: a review of the literature, International Endodontic Journal 40 (2007) 415–426.
[3] R.G. Macedo, P.R. Wesselink, F. Zaccheo, D. Fanali, L.W.M. Van der Sluis, Reaction rate of NaOCl in contact with bovine dentine: effect of activation, exposure time, concentration and pH, International Endodontic Journal 43 (12) (2010) 1108–1115.
[4] W.R. Moorer, P.R. Wesselink, Factors promoting the tissue dissolving capability of sodium hypochlorite, International Endodontic Journal 15 (1982) 187–196.
[5] L.-M. Jiang, B. Verhaagen, M. Versluis, L.W.M. Van der Sluis, The influence of the oscillation direction of an ultrasonic file on the cleaning efficacy of passive ultrasonic irrigation, Journal of Endodontics 36 (8) (2010) 1372–1376.
[6] M. Ahmad, T. Pitt Ford, L. Crum, Ultrasonic debridement of root canals: an insight into the mechanisms involved, Journal of Endodontics 13 (3) (1987) 93–101.
[7] T. Joyce Tiong, G.J. Price, Ultrasound promoted reaction of rhodamine B with sodium hypochlorite using sonochemical and dental ultrasonic instruments, Ultrasonics Sonochemistry 19 (2012) 358–364.
[8] A.D. Walmsley, Ultrasound and root canal treatment: the need for scientific evaluation, International Endodontic Journal 20 (1987) 105–111.
[9] M. Ahmad, T.R. Pitt Ford, L.A. Crum, A.J. Walton, Ultrasonic debridement of root canals: acoustic cavitation and its relevance, Journal of Endodontics 14 (10) (1988) 486–493.
[10] W.R.E. Laird, A.D. Walmsley, Ultrasound in dentistry. Part l – biophysical interactions, Journal of Dentistry 19 (1991) 14–17.
[11] R.A. Roy, M. Ahmad, L.A. Crum, Physical mechanisms governing the hydrodynamic response of an oscillating ultrasonic file, International Endodontic Journal 27 (1994) 197–207.
[12] S.C. Lea, G.J. Price, A.D. Walmsley, A study to determine whether cavitation occurs around dental ultrasonic scaling instruments, Ultrasonics Sonochemistry 12 (2003) 233–236.
[13] B. Felver, D.V. King, S.C. Lea, G.J. Price, A.D. Walmsley, Cavitation occurrence around ultrasonic dental scalers, Ultrasonics Sonochemistry 16 (2009) 692–697.
[14] L.-M. Jiang, B. Verhaagen, M. Versluis, J. Langedijk, P.R. Wesselink, L.W.M. Van der Sluis, The influence of the ultrasonic intensity on the cleaning efficacy of passive ultrasonic irrigation, Journal of Endodontics 37 (5) (2011) 688–692.
[15] C.E. Brennen, Cavitation and Bubble Dynamics, Oxford University Press, 1995.
[16] L.-M. Jiang, B. Verhaagen, M. Versluis, L.W.M. Van der Sluis, Evaluation of a sonic device designed to activate irrigant in the root canal, Journal of Endodontics 36 (1) (2010) 143–146.
[17] R.E.A. Arndt, V.H. Araki, H. Higuchi, Some observations of tip-vortex cavitation, Journal of Fluid Mechanics 229 (1991) 269–289.
[18] F. Hegedüs, C. Hös, Z. Pandula, L. Kullmann, Measurement of the cavitating vortex shedding behind rectangular obstacles, in: 25th IAHR Symposium on Hydraulic Machinery and Systems, IOP Conference Series: Earth and Environmental Science, vol. 12, 2010, p. 012066.
[19] W. Wienken, J. Stiller, A. Keller, A method to predict cavitation inception using large-eddy simulation and its application to the flow past a square cylinder, Journal of Fluids Engineering 218 (2006) 316–325.
[20] P. Kundu, I. Cohen, Fluid mechanics, 3rd Edition., Elsevier Academic Press, San Diego, CA, USA, 2004.
[21] S.C. Lea, A.D. Walmsley, P.J. Lumley, Analyzing endosonic root canal file oscillations: an in vitro evaluation, Journal of Endodontics 36 (5) (2010) 880–883.
[22] B. Verhaagen, C. Boutsioukis, L.W.M. Van der Sluis, M. Versluis, Acoustic streaming induced by ultrasonically oscillating endodontic files, submitted for publication.
[23] K. Suslick, S. Doktycz, E. Flint, On the origin of sonoluminescence and sonochemistry, Ultrasonics 28 (5) (1990) 280–290.
[24] M. Ashokkumar, T.J. Mason, Sonochemistry, John Wiley & Sons, Inc., 2000.
[25] D. Fernandez Rivas, A. Prosperetti, A.G. Zijlstra, D. Lohse, H.J.G.E. Gardeniers, Efficient sonochemistry through microbubbles generated with micromachined surfaces, Angewandte Chemie International Edition 49 (50) (2010) 9699–9701.
[26] D. Fernandez Rivas, B. Verhaagen, J. Seddon, A.G. Zijlstra, L.-M. Jiang, L.W.M. Van der Sluis, A. Prosperetti, M. Versluis, D. Lohse, H.J.G.E. Gardeniers, Localized removal of layers of metal, polymer or biomaterial by cavitating microbubbles, Biomicrofluidics 6 (2012) 034114.
[27] P. Marmottant, M. Versluis, N. De Jong, S. Hilgenfeldt, D. Lohse, High-speed imaging of an ultrasound-driven bubble in contact with a wall: narcissus effect and resolved acoustic streaming, Experiments in Fluids 41 (2006) 147–153.
[28] R.H. Liu, J. Yang, M.Z. Pindera, M. Athavale, P. Grodzinski, Bubble-induced acoustic micromixing, Lab Chip 2 (3) (2002) 151–157.
[29] F. Young, Sonoluminescence from water containing dissolved gases, The Journal of the Acoustical Society of America 60 (1976) 100.
[30] K. Suslick, N. Eddingsaas, D. Flannigan, S. Hopkins, H. Xu, Extreme conditions during multibubble cavitation: sonoluminescence as a spectroscopic probe, Ultrasonics Sonochemistry 18 (4) (2011) 842–846.
[31] D. Lohse, Sonoluminescence–cavitation hots up, Nature 434 (2005) 33–34.
[32] C. Ohl, T. Kurz, R. Geisler, O. Lindau, W. Lauterborn, Bubble dynamics, shock waves and sonoluminescence, Philosophical Transactions of the Royal Society of London Series A: Mathematical, Physical and Engineering Sciences 357 (1751) (1999) 269–294.
[33] S. Hilgenfeldt, S. Grossmann, D. Lohse, A simple explanation of light emission in sonoluminescence, Nature 398 (6726) (1999) 402–405.
[34] S. Hatanaka, H. Mitome, K. Yasui, S. Hayashi, Single-bubble sonochemiluminescence in aqueous luminol solutions, Journal of the American Chemical Society 124 (35) (2002) 10250–10251.
[35] P. Kanthale, M. Ashokkumar, F. Grieser, Sonoluminescence, sonochemistry (H_2O_2 yield) and bubble dynamics: frequency and power effects, Ultrasonics Sonochemistry 15 (2) (2008) 143–150.
[36] E.N. Harvey, Sonoluminescence and sonic chemiluminescence, Journal of the American Chemical Society 61 (9) (1939) 2392–2398.
[37] D. Fernandez Rivas, M. Ashokkumar, T. Leong, K. Yasui, T. Tuziuti, S. Kentish, D. Lohse, H.J. Gardeniers, Sonoluminescence and sonochemiluminescence from a microreactor, Ultrasonics Sonochemistry 19 (2012) 1252–1259.
[38] A. Brotchie, F. Grieser, M. Ashokkumar, Effect of power and frequency on bubble-size distributions in acoustic cavitation, Physical Review Letters 102 (8) (2009) 84302.
[39] J. Lee, M. Ashokkumar, S. Kentish, F. Grieser, Determination of the size distribution of sonoluminescence bubbles in a pulsed acoustic field, Journal of the American Chemical Society 127 (48) (2005) 16810–16811.
[40] H.N. McMurray, B.P. Wilson, Mechanistic and spatial study of ultrasonically induced luminol chemiluminescence, The Journal of Physical Chemistry A 103 (20) (1999) 3955–3962.

[41] R.O. Cleveland, O.A. Sapozhnikov, M.R. Bailey, L.A. Crum, A dual passive cavitation detector for localized detection of lithotripsy-induced cavitation in vitro, Journal of the Acoustical Society of America 107 (3) (2000) 1745–1758.
[42] C.C. Coussios, C.H. Farny, G. ter Haar, R.A. Roy, Role of acoustic cavitation in the delivery and monitoring of cancer treatment by high-intensity focused ultrasound (hifu), International Journal of Hyperthermia 23 (2) (2007) 105–120.
[43] M. Versluis, Review: high-speed imaging, Experiments in Fluids 54 (2) (2013) 1458.
[44] B. Verhaagen, S.C. Lea, L.W.M. van der Sluis, A.D. Walmsley, M. Versluis, Oscillation characteristics of endodontic files: numerical model and its validation, IEEE Transactions on Ultrasonics, Ferroelectrics and Frequency Control 59 (11) (2012) 2448–2459.
[45] D.M. Deng, J.M. Ten Cate, Demineralization of dentin by streptococcus mutans biofilms grown in the constant depth film fermentor, Caries Research 38 (1) (2004) 54–61.
[46] S. Labouret, J. Frohly, Bubble size distribution estimation via void rate dissipation in gas saturated liquid. Application to ultrasonic cavitation bubble fields, The European Physical Journal Applied Physics 19 (1) (2002) 39–54.
[47] L.W.M. Van der Sluis, M.P.J.M. Vogels, B. Verhaagen, R.G. Macedo, P.R. Wesselink, Study on the influence of refreshment/activation cycles and irrigants on mechanical cleaning efficiency during ultrasonic activation of the irrigant, Journal of Endodontics 36 (4) (2010) 737–740.
[48] M. Wall, M. Ashokkumar, R. Tronson, F. Grieser, Multibubble sonoluminescence in aqueous salt solutions, Ultrasonics Sonochemistry 6 (1999) 7–14.
[49] Z. Zeravcic, D. Lohse, W. van Saarloos, Collective oscillations in bubble clouds, Journal of Fluid Mechanics 680 (2011) 114–149.
[50] S. Hatanaka, K. Yasui, T. Kozuka, T. Tuziuti, H. Mitome, Influence of bubble clustering on multibubble sonoluminescence, Ultrasonics 40 (1–8) (2002) 655–660.
[51] K. Yasui, Y. Iida, T. Tuziuti, T. Kozuka, A. Towata, Strongly interacting bubbles under an ultrasonic horn, Physical Review E 77 (1) (2008) 016609.
[52] K. Yasui, T. Tuziuti, Y. Iida, Optimum bubble temperature for the sonochemical production of oxidants, Ultrasonics 42 (1) (2004) 579–584.
[53] K. Yasui, A. Towata, T. Tuziuti, T. Kozuka, K. Kato, Effect of static pressure on acoustic energy radiated by cavitation bubbles in viscous liquids under ultrasound, The Journal of the Acoustical Society of America 130 (5) (2011) 3233–3242.
[54] M. Ashokkumar, J. Lee, Y. Iida, K. Yasui, T. Kozuka, T. Tuziuti, A. Towata, Spatial distribution of acoustic cavitation bubbles at different ultrasound frequencies, ChemPhysChem 11 (8) (2010) 1680–1684.
[55] Y. Didenko, D. Nastich, S. Pugach, Y. Polovinka, V. Kvochka, The effect of bulk solution temperature on the intensity and spectra of water sonoluminescence, Ultrasonics 32 (1) (1994) 71–76.
[56] D. Flannigan, K. Suslick, Plasma formation and temperature measurement during single-bubble cavitation, Nature 434 (7029) (2005) 52–55.
[57] E. Flint, K. Suslick, The temperature of cavitation, Science 253 (5026) (1991) 1397.
[58] K. Okitsu, T. Suzuki, N. Takenaka, H. Bandow, R. Nishimura, Y. Maeda, Acoustic multibubble cavitation in water: a new aspect of the effect of a rare gas atmosphere on bubble temperature and its relevance to sonochemistry, The Journal of Physical Chemistry B 110 (41) (2006) 20081–20084.
[59] C. Dekerckheer, K. Bartik, J.-P. Lecomte, J. Reisse, Pulsed sonochemistry, The Journal of Physical Chemistry A 102 (46) (1998) 9177–9182.
[60] D. Fernandez Rivas, L. Stricker, A.G. Zijlstra, H.J.G.E. Gardeniers, D. Lohse, A. Prosperetti, Ultrasound artificially nucleated bubbles and their sonochemical radical production, Ultrasonics Sonochemistry 20 (1) (2013) 510–524.
[61] Y. Iida, K. Yasui, T. Tuziuti, Sivakumar, Ultrasonic cavitation in microspace, Chemical Communications (2004) 2280–2281.
[62] C. Boutsioukis, B. Verhaagen, A.D. Walmsley, M. Versluis, L.W.M. Van der Sluis, Measurement and visualization of file-to-wall contact during ultrasonically activated irrigation in vitro, International Endodontic Journal, in press, http://dx.doi.org/2010.1111/iej.12097.
[63] D. Krefting, R. Mettin, W. Lauterborn, High-speed observation of acoustic cavitation erosion in multibubble systems, Ultrasonics Sonochemistry 11 (2004) 119–123.
[64] T.J.C. Terwisga, P.A. Fitzsimmons, L. Ziru, E.J. Foeth, Cavitation erosion – a review of physical mechanisms and erosion risk models, in: Proceedings of the 7th International Symposium on Cavitation CAV2009, 2009, pp. 1–13.
[65] E.-A. Brujan, K. Nahen, P. Schmidt, A. Vogel, Dynamics of laser-induced cavitation bubbles near an elastic boundary, Journal of Fluid Mechanics 433 (2001) 251–281.
[66] Personal communication with several endodontists.
[67] A. Henglein, R. Ulrich, J. Lilie, Luminescence and chemical action by pulsed ultrasound, Journal of American Chemical Society 111 (6) (1989) 1974–1979.
[68] T. Tuziuti, K. Yasui, T. Kozuka, A. Towata, Influence of liquid-surface vibration on sonochemiluminescence intensity, The Journal of Physical Chemistry A 114 (27) (2010) 7321–7325.
[69] S.L. Lea, G.J. Price, A.D. Walmsley, A study to determine whether cavitation occurs around dental ultrasonic scaling instruments, Ultrasonics Sonochemistry 12 (2005) 233–236.
[70] R.G. Macedo, S.I. Nikitenko, B. Verhaagen, D. Fernandez Rivas, J.G.E. Gardeniers, M. Versluis, L.W.M. Van der Sluis, Sonochemical dosimetry with iso-butyl nitrite and its potential application in, dental research, submitted for publication.